

Design, theory, and measurement of a polarization-insensitive absorber for terahertz imaging

N. I. Landy,¹ C. M. Bingham,¹ T. Tyler,² N. Jokerst,² D. R. Smith,² and W. J. Padilla¹

¹*Department of Physics, Boston College, 140 Commonwealth Avenue, Chestnut Hill, Massachusetts 02467, USA*

²*Department of Electrical and Computer Engineering, Duke University, Durham, North Carolina 27708, USA*

(Received 28 July 2008; revised manuscript received 21 January 2009; published 5 March 2009)

We present the theory, design, and realization of a polarization-insensitive metamaterial absorber for terahertz frequencies. Effective-medium theory is used to describe the absorptive properties of the metamaterial in terms of optical constants—a description that has been thus far lacking. From our theoretical approach, we construct a device that yields over 95% absorption in simulation. Our fabricated design consists of a planar single unit-cell layer of metamaterial and reaches an absorptivity of 77% at 1.145 THz.

DOI: [10.1103/PhysRevB.79.125104](https://doi.org/10.1103/PhysRevB.79.125104)

PACS number(s): 78.20.Bh, 78.20.Ci

I. INTRODUCTION

The advent of terahertz (THz) spectroscopy has ushered in a new field of research as scientists seek to exploit the electromagnetic signatures of materials in the THz range of the spectrum. Specifically, the ability to perform imaging in THz would have profound impact on the areas of security,^{1–4} biology,^{5,6} and chemistry.^{7,8} However, imaging in terahertz is complicated by the lack of easily accessible electromagnetic responses from naturally occurring materials.^{9,10}

Electromagnetic metamaterials (MMs) (Refs. 11 and 12) are one potential solution to overcome this “THz gap.”¹³ The operational frequency of a given MM design is geometrically scalable to other regimes of the electromagnetic spectrum. Various MM structures have been shown to naturally couple to either the electric and/or magnetic components of light in frequency ranges from radio,¹⁴ microwave,¹⁵ millimeter wave,¹⁶ THz,¹³ midinfrared (MIR),¹⁷ near infrared (NIR),¹⁸ to the near optical.¹⁹ A great deal of effort has been exerted to create low-loss metamaterial devices such as negative index (NI) structures¹⁵ and electromagnetic cloaks.^{20,21} However, the substantial loss tangent that occurs at the center frequencies of metamaterial resonances can be exploited as well. This resonant loss phenomenon serves as the starting point for the investigation of MMs as narrow-band absorbing elements for thermal imaging devices.

We present the theory, design, fabrication, and measurement of a single-frequency metamaterial absorbing element. By using the effective-medium model, we are able to demonstrate the ideal absorber—a material that does not have to be a certain fraction of the operational wavelength to function.²² We demonstrate that the proper design of an absorber requires independent control of four parameters: the real and imaginary components of both effective optical constants. This demonstrates that a characterization in terms of a single parameter, such as the sheet resistance,²³ is incomplete.

The simulated design reaches a peak absorptivity of 95% at 1.13 THz and the fabricated structure reaches a measured absorptivity of 65% at 1.145 THz. This absorptivity is comparable to existing MM absorber designs,^{24,25} but our design is also polarization insensitive, which maximizes the absorption of light.

II. THEORY

The absorptivity $A(\omega)$ of a material is given by the transmission $T(\omega)$ and reflectance $R(\omega)$ as $A(\omega) = 1 - T(\omega) - R(\omega)$. In terms of the complex transmissivity (\tilde{t}) and reflectivity (\tilde{r}), this can be written as $A = 1 - |\tilde{t}(\omega)|^2 - |\tilde{r}(\omega)|^2$. Therefore, $A = 1$ when $T = R = 0$. In Ref. 26, the frequency-dependent transmissivity $\tilde{t}(\omega)$ was determined to be dependent on the complex index of refraction $\tilde{n}(\omega) = n_1 + in_2$ and impedance $\tilde{Z}(\omega) = Z_1 + iZ_2$ for a slab of length d as

$$t(\omega)^{-1} = \left[\sin(\tilde{n}kd) - \frac{i}{2} \left(\tilde{Z} + \frac{1}{\tilde{Z}} \right) \cos(\tilde{n}kd) \right] e^{ikd}. \quad (1)$$

where $k = \omega/c$ and c is the speed of light in the vacuum. We use the convention where a subscripted 1 and 2 denote the real and imaginary parts of a complex function, respectively.

As \tilde{Z} approaches unity (the free space value), the reflectivity will drop to zero and the transmissivity will be determined entirely by \tilde{n} as follows:

$$t^{-1} = [\sin(\tilde{n}kd) - i \cos(\tilde{n}kd)] e^{ikd}. \quad (2)$$

Upon substitution of the exponential forms this becomes

$$t^{-1} = e^{-i(n_1-1)kd} e^{n_2kd}. \quad (3)$$

So the transmission ($T = |\tilde{t}|^2$) is

$$T = e^{-2n_2kd}. \quad (4)$$

Therefore, as n_2 approaches infinity (for a given d),

$$\lim_{n_2 \rightarrow \infty} T = 0. \quad (5)$$

The combined dielectric and magnetic losses in the system are characterized by n_2 . Therefore the physical interpretation of the above derivation is that (in the absence of reflections) the transmission of an electromagnetic wave with a wave vector k through a slab of thickness d is determined entirely by losses in the slab. To create a very high absorber it is then necessary for $\tilde{Z} = 1$ at a point where n_2 is large. The higher the value of n_2 that can be obtained, the thinner the slab can be in the propagation direction. In this manner, one can overcome the quarter-wavelength thickness requirement of traditional Salisbury screens and Jaumann absorbers.^{22,27}

Precise control of \tilde{n} and \tilde{Z} is necessary to realize a high absorber. Electromagnetic MMs are prime candidates for this task since they can be designed to couple to electric and magnetic components of light. This enables precise tuning of the complex frequency-dependent permittivity $\tilde{\epsilon}(\omega)$ and permeability $\tilde{\mu}(\omega)$ of a MM slab. The index \tilde{n} and impedance \tilde{Z} are in turn given by $\tilde{n}(\omega) = \sqrt{\tilde{\epsilon}(\omega)\tilde{\mu}(\omega)}$ and $\tilde{Z}(\omega) = \sqrt{\tilde{\mu}(\omega)/\tilde{\epsilon}(\omega)}$.

MMs are typically highly resonant in $\tilde{\epsilon}$ and/or $\tilde{\mu}$, where the relevant optical constants approximate the form of a complex oscillator in frequency,

$$\epsilon(\omega), \mu(\omega) = \epsilon_\infty, \mu_\infty + \frac{F_{\epsilon, \mu} \omega^2}{\omega_{0\epsilon, \mu}^2 - \omega^2 - i\gamma\omega}, \quad (6)$$

where F is the oscillator strength, γ is the damping, ω_0 is the center frequency of the oscillator, and $\epsilon_\infty, \mu_\infty$ are high-frequency contributions to ϵ, μ . This form for an oscillator describes the frequency response of metamaterials and we term this a ‘‘Pendrian’’ after Ref. 12.

We consider a single-frequency operation point, defined by ω_0 , for two oscillators with identical frequency dependence such that $\tilde{\epsilon}(\omega) = \tilde{\mu}(\omega)$; then $\tilde{Z}(\omega_0) = 1$ and $n_2(\omega_0)$ is maximized with a value of

$$n_2(\omega_0) = \frac{F\omega_0}{\gamma} \quad (7)$$

which, according to Eq. (4), yields

$$A(\omega_0) = 1 - e^{2(F\omega_0^2 d/c\gamma)}. \quad (8)$$

For the more realistic case, when $\epsilon_\infty \neq \mu_\infty$, then $\tilde{Z}(\omega_0) \neq 1$ and A is no longer determined solely by n_2 . However, for large n_2 , $T(\omega_0)$ remains low and $R(\omega_0)$ can be written approximately in terms of $Z(\omega)$ (Ref. 26) such that

$$R(\omega_0) = \left(\frac{Z(\omega_0) - 1}{Z(\omega_0) + 1} \right)^2. \quad (9)$$

Regardless of ϵ_∞ and μ_∞ , an optimal narrow-band absorber must maximize F with respect to γ in both ϵ and μ . F is determined by the geometry, filling factor, and conductivity of the two metallizations. γ is determined by losses in the metallization and substrate. The optimal absorber will then use the MM geometries with the maximum possible filling factor. Furthermore, metallization and substrate should be chosen to minimize losses at the operation frequency as determined by Eq. (7) above.

III. DESIGN

From a theoretical viewpoint, it would seem simple to design a MM that would provide such a response in ϵ and μ . However, there are several complications to the theoretical analysis presented above due to the specific properties of MMs. For instance, the periodicity inherent to most MMs contributes to spatial dispersion, i.e., $\epsilon = \epsilon(\omega, \mathbf{k})$ and $\mu = \mu(\omega, \mathbf{k})$.²⁸ This spatial dispersion causes the optical parameters to deviate from the pure form of Eq. (6). Spatial dis-

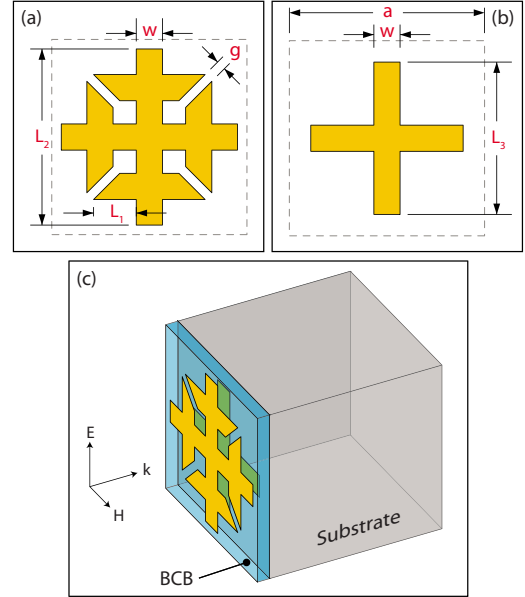


FIG. 1. (Color online) (a) ERR, (b) cross, and (c) combined ERR and cross. The dimensions in microns are $a=84$, $L_1=52.5$, $L_2=74$, $L_3=64$, $w=11$, and $g=4$. Axes indicate the wave polarization and propagation direction.

persion also causes antiresonances in $\tilde{\mu}(\tilde{\epsilon})$ due to resonances in $\tilde{\epsilon}(\tilde{\mu})$.²⁹ Additionally, conventional electric^{30,31} and magnetic¹⁵ MMs are highly coupled when they share a center resonant frequency.³² Typically, electric metamaterials have higher-order electric resonances, and thus in general one does not necessarily have the condition that $\epsilon_\infty = \mu_\infty$, leading to a nonzero reflectivity as described above. In our particular case for the design of a narrow-band high absorber, a solution to the latter problem was to use the low-frequency LC resonance to lower ϵ_∞ at the operational frequency, and then use to higher-frequency side-length response to match $\tilde{\mu}$ at the operational frequency.

The electric responses were provided by a modified electrically coupled ring resonator (ERR) shown schematically in Fig. 1(a). The ERR chosen had fourfold rotational symmetry about the propagation axis and was therefore polarization insensitive.³⁰ The lower-frequency electric response used to tune the $\epsilon(\omega)$ curve was driven by the LC loop in the ERR. The higher-frequency response used to couple to $\epsilon(\omega)$ was created by the dipolelike interaction of the metallizations in adjacent unit cells.

The magnetic response was created by combining the ERR with a cross structure [Fig. 1(b)] in a parallel structure separated by a layer of benzocyclobutane (BCB) [Fig. 1(c)]. The magnetic component \mathbf{H} of a TEM wave coupled to the center stalks of the two metallizations that were perpendicular to the propagation vector, such that antiparallel currents were driven. A polarization-sensitive design based on similar parameters has been shown at both THz (Ref. 25) and microwave²⁴ frequencies.

Practical realization of metamaterials dictates the use of a support substrate that complicates the theoretical optimization of the structure. This substrate is typically thick in the propagation direction compared to the thickness of the

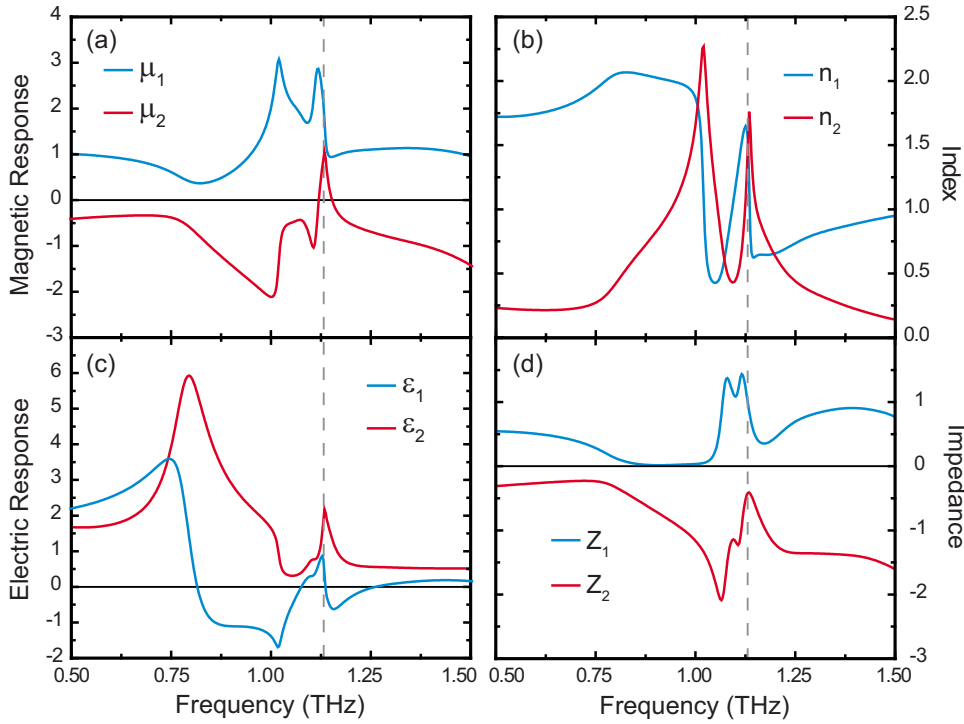


FIG. 2. (Color online) Real (black, blue online) and imaginary (dark gray, red online) components of (a) μ and (c) ϵ . Real (black, blue online) and imaginary (dark gray, red online) components of (b) n and (d) Z . The vertical dashed line indicates the frequency of maximum absorptivity.

metamaterial and the lateral unit-cell dimensions. This supporting structure introduces ambiguity in the definition of the unit cell as well as significant asymmetry in the propagation direction, both of which complicate the definition of Z_{eff} and n_{eff} .³³ However, some portions of the substrate must be included in simulation because it has a measurable effect on the form of the MM resonances due to the dielectric of the substrate, ϵ_s .³⁴

The effect of the substrate on the MM's resonances can be shown directly in simulation. A parameter sweep of the substrate thickness d shows that the effect of the added dielectric on the MM resonance saturates near a value of $d=d_s$. For $d>d_s$, the only added effect is a factor $\exp[i\sqrt{\epsilon_s}k(\omega)(d-d_s)]$ to $\tilde{\mu}(\omega)$, so long as we are far in frequency from Fabry-Perot resonances. As substrates are typically chosen for low loss in the frequency range of interest, $|\tilde{\mu}(\omega)|$ is virtually unchanged and the extended substrate only adds phase. The appropriate unit-cell boundary in the propagation direction is therefore given by d_s and the MM elements on the substrate. The impedance mismatch at the MM-substrate and substrate-air boundaries can then be incorporated into the homogenized effective medium as these boundaries are within the unit cell.

The extracted optical constants for the metamaterial absorber shown in Fig. 1 are plotted in Fig. 2. The real and imaginary components $\tilde{\epsilon}$ and $\tilde{\mu}$, as plotted in Figs. 2(a) and 2(c), are complicated by the effects of spatial dispersion, as previously mentioned. However, various features of the plots enable interpretation of the forms of these curves. The lowest-frequency feature in ϵ_2 at $\omega=800$ GHz, shown in Fig. 2(c), is the conventional MM electrically coupled inductive-capacitive resonance of the ERR. Notice that this is accompanied by an antiresonance in $\tilde{\mu}(\omega)$, which is characterized by a negative imaginary component that peaks at the center frequency of $\epsilon_1(\omega)$, defined by the cusp near ω

$=1.02$ THz. A second electric resonance appears at approximately $\omega=1.125$ THz due to the cut-wire response of the cross. This is accompanied by an antiresonance in $\tilde{\mu}(\omega)$ centered at the same frequency. The resonance in $\tilde{\mu}(\omega)$ is weak relative to the neighboring resonances in ϵ and thus difficult to observe. However, μ_2 has a distinct positive peak at 1.13 THz. This, combined with an approximately Pendriam curve in μ_1 , indicates the presence of a magnetic response centered at this frequency. There is also a small but distinct kink in $\tilde{\epsilon}(\omega)$ due to the antiresonance caused by the magnetic response.

Even though the forms of ϵ and μ are complicated by several resonances and antiresonances, the form of n and z directly determine the form of R , T , and A . Therefore, R , T , and A in Fig. 3 do not show the same complicated behavior as the optical constants in Fig. 2. Figure 2(b) shows the

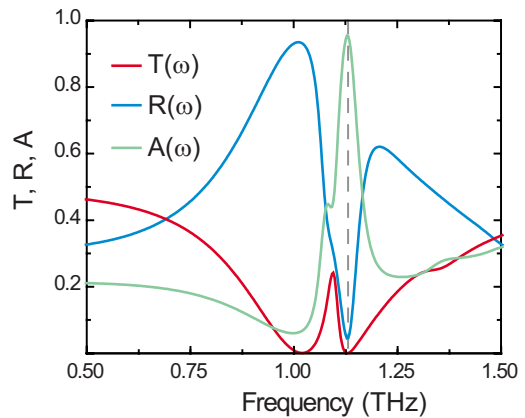


FIG. 3. (Color online) Reflectance (black, blue online), transmission (dark gray, red online), and absorptivity (light gray, green online) for the simulated absorber. The vertical dashed line indicates the frequency of maximum absorptivity.

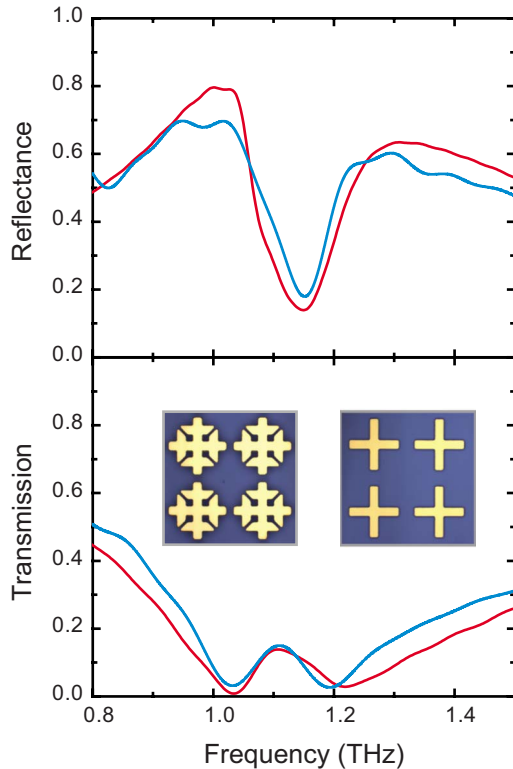


FIG. 4. (Color online) Reflectance and transmission results for experiment (black, blue online) and simulation (dark gray, red online).

refractive index $\tilde{n}(\omega)$ and Fig. 2(d) shows impedance $\tilde{Z}(\omega)$ and demonstrates how close the structure approximates an ideal absorber. At 1.13 THz the real impedance is near unity, $Z_1 \sim 1$, and the complex impedance Z_2 is minimized, such that $R \sim 0$. As desired, the imaginary index n_2 is maximized near a value of ~ 1.75 , which minimizes T . This results in a peak absorptivity of 95%, plotted as the gray (green online) solid curve shown in Fig. 3.

IV. FABRICATION AND EXPERIMENT

The two-layer metallization MM absorber sample was fabricated on a high-resistivity 1-mm-thick silicon substrate. A 3- μm -thick SiO_2 layer was deposited on the Si substrate using plasma-enhanced chemical vapor deposition (PECVD). The bottom cross-shaped metallization (30 nm Ti/40 nm Pt adhesion layer and 200 nm Au layer) was patterned using standard negative lithography, metal evaporation, and metal liftoff. The BCB dielectric (Cyclotene 3022–46, Dow) was deposited using two consecutive spin-coat depositions and soft cures in a vacuum oven, resulting in a final thickness of approximately 6 μm . The top ERR metallization layer structure and patterning used the same process as that of the cross. The two unit cells (one for each layer) are shown as the insets to the bottom panel of Fig. 4.

The MM absorber sample was examined experimentally using a Fourier-transform infrared (FTIR) spectrometer. Polarized light from a mercury arc lamp was transmitted and reflected from both the sample and a reference substrate, and

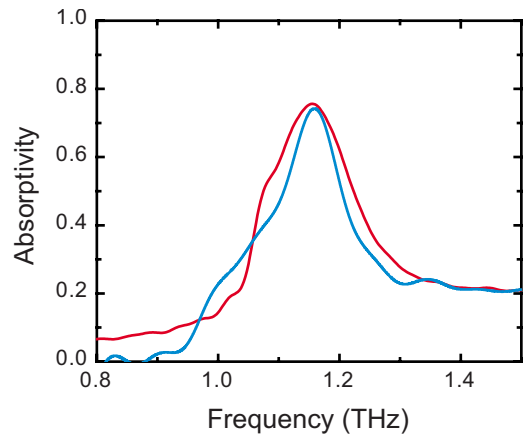


FIG. 5. (Color online) Experimental (black, blue online) and simulated (dark gray, red online) absorptivity curves.

then focused on the detector, a liquid-helium-cooled Si bolometer. Measurements of the sample for both polarizations were characterized and we found no deviations within experimental error. Measured $T(\omega)$ and $R(\omega)$ were used to calculate the experimental $A(\omega)$.

Fabrication tolerances in the structures resulted in some deviation from the theoretically optimized case and are shown in Fig. 4. The corners of the ERR and cross structures are slightly rounded and the BCB thickness was 6 μm rather than the optimal 5.8 μm . All of these factors were incorporated into the computer model and the resimulated transmission and reflection for the metamaterial absorber are shown in Fig. 4, with the experimental measurement of $T(\omega)$ and $R(\omega)$, and absorption is shown in Fig. 5. In comparison to the theoretically optimized structure results shown in Fig. 3, the fabricated sample exhibits a shift in the MM resonances. The first transmissive minimum has shifted by 10 GHz, while the second minimum has shifted by 54 GHz, both to higher frequencies. The minimum in reflectance has shifted from 1.128 THz to 1.15 THz. This is expected as electric responses are sensitive to metallic structure rounding²¹ and the thickness of the BCB layer partially determines the magnetic coupling. However, this change in geometrical parameters does not fully account for the disagreement between Figs. 3 and 4.

We compare our experimental data to simulation results shown in Fig. 3. At 0.8 THz, $T(\omega)$ and $R(\omega)$ are well matched in experiment and simulation, but the forms deviate as the curves approach the MM resonances. The experimental reflectivity reaches a minimum of only 18% compared to the simulated value of 2%. Likewise, the first and second transmissive minima reach values of 3% and 3%, respectively, as opposed to less than 0.1% in our initial simulation. Several mechanisms may be behind this disparity.

The off-resonant agreement indicates that the discrepancies are related to resonant forms of the constitutive parameters $\tilde{\epsilon}$ and $\tilde{\mu}$. As indicated by Eq. (7) lowering F or increasing γ of the resonances translates into a higher minimum in $T(\omega)$ as the peak value of the effective loss (n_2) is decreased. This also changes the form of $\tilde{Z}(\omega)$ and therefore the form of $R(\omega)$.

For both the electric and magnetic resonances, γ is primarily determined by the loss in the BCB substrate between the ERR and cross. Previous work has determined that dielectric losses are the primary mechanism and may be 1 order of magnitude greater than Ohmic loss.²⁴ Also, because BCB is the primary dielectric that tunes the capacitance of each structure, any deviation from the nominal value of $\epsilon=2.5+0.0125i$ will lead to variation in absorbance. Further, it is well known that the dielectric value of many polymer compounds has significant dependence on frequency, especially within the THz range.³⁵ As previously mentioned, the “strength of the oscillator” F is determined by the geometry, filling fraction, and conductivity of the two metallizations. Therefore, the deviation of experimental curves in Fig. 4 may be caused by a combination of increased loss in the BCB and lowered conductivity in the metallizations.

The best fit of simulation to experimental data is shown in Figs. 4 and 5. The loss tangent of BCB was found to be approximately 1 order of magnitude greater than the nominal value, while the conductivity of gold was found to have decreased 1 order of magnitude. In simulation, the different dielectric constants changed the form of the reflected and transmitted pulses, which complicated etalon removal in the time domain. This resulted in the oscillatory behavior in Fig. 4. As a consequence of the nonuniform shift of both the magnetic and electric resonances, as well as increased damping due to loss, \tilde{n} and \tilde{Z} have deviated from their optimum values, resulting in a peak absorptivity of 77% (Fig. 5).

V. DISCUSSION AND CONCLUSIONS

We now discuss the potential use of the metamaterial absorber as a thermal imager for the THz frequency range. Compared to existing THz absorbers used for bolometric detection, our device is narrow band. This enables spectrally

selective applications, such as in the detection of explosives. As previously mentioned, existing resonant absorbers are fundamentally limited to quarter-wavelength thicknesses. Our design is not limited in this fashion and the thickness can be optimized for thermal detection. However, unlike previous MM absorber designs,²⁵ our device is polarization insensitive. This may be ideal for certain applications, as it maximizes absorption for arbitrarily polarized or incoherent light. As a MM device, our design is geometrically scalable to different frequency ranges. This scalability is limited only by limitations in fabrication and loss in constituent materials. Other absorbing devices lack this scalability.³⁶ The limitations of the narrow-band resonant design could be overcome by using multiple distinct unit cells³⁷ or by incorporating tunable or frequency agile metamaterial components.³⁸

It should be noted that designs presented here are bianisotropic—a result of asymmetry in the propagation direction—and belong to Shoenflies point group C_4 .³⁹ We have performed simulations (not shown) in order to elucidate the impact of the bianisotropy on absorptive properties of the metamaterial. We studied the cross polarization in transmission as a function of frequency for the design shown in Fig. 1. Computer simulations indicate that the cross polarization is small and achieves a maximum of only 10^{-4} over the frequency range of interest. We also investigated the cross polarizations for designs presented in Refs. 24 and 25 and found similar results. Thus, for normal-incidence radiation, the effect of bianisotropy is negligible.

In conclusion, we have derived general conditions to create an absorber based on effective-medium theory and for the specific case of MM elements. We have shown that such a design can reach absorptivities approaching unity within a narrow band. We have also successfully implemented this approach with a THz frequency absorber design. The theory presented here and the design specifically show a great promise to create absorbers at any decade of frequency.

-
- ¹F. Oliveira, R. Barat, B. Schulkin, J. F. Federici, D. Gary, and D. A. Zimdars, Proc. SPIE **5070**, 60 (2003).
²D. A. Zimdars, Proc. SPIE **5070**, 108 (2003).
³Hai-Bo Liu, Yunqing Chen, Glenn J. Bastiaans, and X.-C. Zhang, Opt. Express **14**, 415 (2006).
⁴J. Barber, D. E. Hooks, D. J. Funk, R. D. Averitt, A. J. Taylor, and D. Babikov, J. Phys. Chem. A **109**, 3501 (2005).
⁵X.-C. Zhang, Phys. Med. Biol. **47**, 3667 (2002).
⁶T. R. Globus, D. L. Woolard, T. Khromova, T. W. Crowe, M. Bykhovskaia, B. L. Gelmont, J. L. Hesler, and A. C. Samuels, J. Biol. Phys. **29**, 89 (2003).
⁷R. H. Jacobsen, D. M. Mittleman, and M. C. Nuss, Opt. Lett. **21**, 2011 (1996).
⁸D. M. Mittleman, J. Cunningham, M. C. Nuss, and M. Geva, Appl. Phys. Lett. **71**, 16 (1997).
⁹G. P. Williams, Rep. Prog. Phys. **69**, 301 (2006).
¹⁰M. Tonouchi, Nat. Photonics **1**, 97 (2007).
¹¹J. B. Pendry, A. J. Holden, W. J. Stewart, and I. Youngs, Phys. Rev. Lett. **76**, 4773 (1996).
¹²J. B. Pendry, A. J. Holden, D. J. Robbins, and W. J. Stewart, IEEE Trans. Microwave Theory Tech. **47**, 2075 (1999).
¹³T. J. Yen, W. J. Padilla, N. Fang, D. C. Vier, D. R. Smith, J. B. Pendry, D. N. Basov, and X. Zhang, Science **303**, 1494 (2004).
¹⁴M. C. K. Wiltshire, J. B. Pendry, I. R. Young, D. J. Larkman, D. J. Gilderdale, and J. V. Hajnal, Science **291**, 849 (2001).
¹⁵D. R. Smith, W. J. Padilla, D. C. Vier, S. C. Nemat-Nasser, and S. Schultz, Phys. Rev. Lett. **84**, 4184 (2000).
¹⁶M. Gokkavas, K. Guven, I. Bulu, K. Aydin, R. S. Penciu, M. Kafesaki, C. M. Soukoulis, and E. Ozbay, Phys. Rev. B **73**, 193103 (2006).
¹⁷S. Linden, C. Enkrich, M. Wegener, J. Zhou, T. Koschny, and C. M. Soukoulis, Science **306**, 1351 (2004).
¹⁸S. Zhang, W. Fan, N. C. Panoiu, K. J. Malloy, R. M. Osgood, and S. R. J. Brueck, Phys. Rev. Lett. **95**, 137404 (2005).
¹⁹G. Dolling, M. Wegener, C. M. Soukoulis, and S. Linden, Opt. Lett. **32**, 53 (2007).
²⁰J. B. Pendry, D. Schurig, and D. R. Smith, Science **312**, 1780 (2006).

- ²¹D. Schurig, J. J. Mock, B. J. Justice, S. A. Cummer, J. B. Pendry, A. F. Starr, and D. R. Smith, *Science* **314**, 977 (2006).
- ²²B. A. Munk, J. B. Pryor, and Y. B. Gan, *Electromagnetic Materials Proc. of the Symposium F, 2003* (World Scientific Publishing Company, Singapore, 2004), p. 977.
- ²³Q. Gao, Y. Yin, D.-B. Yan, and N.-C. Yuan, *Electron. Lett.* **41**, 936 (2005).
- ²⁴N. I. Landy, S. Sajuyigbe, J. J. Mock, D. R. Smith, and W. J. Padilla, *Phys. Rev. Lett.* **100**, 207402 (2008).
- ²⁵H. Tao, N. I. Landy, C. M. Bingham, X. Zhan, R. D. Averitt, and W. J. Padilla, *Opt. Express* **16**, 7181 (2008).
- ²⁶D. R. Smith, D. C. Vier, T. Koschny, and C. M. Soukoulis, *Phys. Rev. E* **71**, 036617 (2005).
- ²⁷A. J. Gatesman, A. Danylov, T. M. Goyette, J. C. Dickinson, R. H. Giles, W. Goodhue, J. Waldman, W. E. Nixon, and W. Hoen, *Proc. SPIE* **6212**, 62120E (2006).
- ²⁸A. Serdyukov, I. Semchenko, S. Tretyakov, and A. Sihvola, *Electromagnetics of Bi-anisotropic Materials: Theory and Applications* (Gordon and Breach, New York, 2001).
- ²⁹R. Liu, T. J. Cui, D. Huang, B. Zhao, and D. R. Smith, *Phys. Rev. E* **76**, 026606 (2007).
- ³⁰W. J. Padilla, M. T. Aronsson, C. Highstrete, M. Lee, A. J. Taylor, and R. D. Averitt, *Phys. Rev. B* **75**, 041102(R) (2007).
- ³¹D. Schurig, J. J. Mock, and D. R. Smith, *Appl. Phys. Lett.* **88**, 041109 (2006).
- ³²D. R. Smith, J. Gollub, J. J. Mock, W. J. Padilla, and D. Schurig, *J. Appl. Phys.* **100**, 024507 (2006).
- ³³C. R. Simovski and S. A. Tretyakov, *Phys. Rev. B* **75**, 195111 (2007).
- ³⁴W. J. Padilla, D. R. Smith, and D. Basov, *J. Opt. Soc. Am. B* **23**, 404 (2006).
- ³⁵H. Tao, A. C. Strikwerda, K. Fan, C. M. Bingham, W. J. Padilla, X. Zhang, and R. D. Averitt, *J. Phys. D* **41**, 232004 (2008).
- ³⁶T. V. Teperik, F. J. Garcia de Abajo, A. G. Borisov, M. Abdelsalam, P. N. Bartlett, Y. Sugawara, and J. J. Baumberg, *Nat. Photonics* **2**, 299 (2008).
- ³⁷Christopher M. Bingham, Hu Tao, Xianliang Liu, Richard D. Averitt, Xin Zhang, and Willie J. Padilla, *Opt. Express* **16**, 18565 (2008).
- ³⁸H.-T. Chen, J. F. O'Hara, A. K. Azad, A. J. Taylor, R. D. Averitt, D. B. Shrekenhamer, and W. J. Padilla, *Nat. Photonics* **2**, 295 (2008).
- ³⁹W. J. Padilla, *Opt. Express* **15**, 1639 (2007).